

# Multi-loop control of stand-alone inverters with minimum number of sensors

ISSN 1755-4535

Received on 14th January 2016

Revised on 18th May 2016

Accepted on 22nd June 2016

doi: 10.1049/iet-pel.2016.0036

www.ietdl.org

Reza Razi, Mohammad Monfared ✉

Department of Electrical Engineering, Faculty of Engineering, Ferdowsi University of Mashhad, Mashhad 91779-48974, Iran

✉ E-mail: m.monfared@um.ac.ir

**Abstract:** This study deals with the design of a load sensorless multi-loop control system for the stand-alone inverter. In the proposed strategy, only the inverter current is measured, which is practically required for both control and protection purposes, then the load voltage and current are both estimated using the linear Kalman filter algorithm, and the gradient descent adaptive control method, respectively. The estimated quantities are used as feedback signals of an inner-outer double-loop controller, which uses a proportional-resonant outer-controller to regulate the output voltage with minimum steady-state error and a simple proportional inner-controller to provide active damping and improve the transient performance. The controller parameters are designed in the frequency domain based on the required bandwidth and stability margin. Furthermore, the controllability and observability, as well as the stability of overall digital control system, including the dynamics of estimators, are analytically investigated. Simulation and experimental results, with a 600 VA prototype, confirm the theoretical achievements and illustrate the excellent performance of the proposed estimation and control scheme.

## 1 Introduction

Distributed generation (DG) systems have attracted a lot of attentions these days. Usually, a power electronic converter is utilised to regulate the generated energy from DGs. In grid-connected inverters, the DG unit acts as a controlled current source, while in an islanded or stand-alone operation mode, the DG unit is the source of power for local loads, and acts as a controlled voltage source [1, 2]. Thus, in islanded operation mode, the inverter should be able to support the local network with the appropriate voltage and frequency. Various control methods for stand-alone inverters are available in the literature, which can be classified into: repetitive control [3, 4], dead-beat [5, 6] and model predictive control (MPC) [7, 8], robust control, such as H-infinity [9] and  $\mu$  synthesis control [10], non-linear control, such as sliding mode [11] and neural network control [12], and model based instantaneous feedback control [13–16].

Repetitive control is specifically interesting in dealing with periodic signals and can successfully reduce the periodic harmonic distortions, while a large memory requirement, and poor performance to non-periodic disturbances are attributed as its major shortcomings [1, 3]. MPC has a relatively simple concept, but as the name implies, requires an accurate model of the converter system. This method is flexible and provides a fast dynamic response [7–9]. The approaches based on robust control theory can systematically handle the possible uncertainties in the system and provide good trade-offs between performance and stability margin. However, they are rather difficult to be implemented on digital processors and design specifications of them are complex [9]. Non-linear controllers present an excellent dynamic performance, and prevent overshoot and ringing in the output waveforms, but these techniques have some major drawbacks, such as complexity, sensitivity to parameter variations, and steady-state errors [2, 16].

In practice, the model based instantaneous feedback control is widely accepted in industrial solutions, which can be realised either single-loop or multi-loop. The single-loop controller employs a voltage regulator with an additional resistor in the filter circuit, which is intended to prevent possible resonances of the LC filter with harmonic components generated by the inverter switching.

While being simple, the single-loop control with passive damping suffers from additional losses of the damping resistor.

On the other hand, the active damping method uses a multi-loop control, in which the additional control loop plays the role of the virtual resistance for damping the resonance oscillations, and at the same time, improving the system stability and dynamic performance [17].

A major drawback associated to multi-loop control schemes is the need for several sensor circuits necessary for measuring all controlled quantities in the nested control loops [15, 16].

Several estimation schemes have been already proposed in literature to replace some measurement circuits with software algorithms [13, 14, 16]. A work by Ahmed *et al.*, showed promising results in this direction of research [13], where only the load current is measured and the load voltage, and the capacitor current, as the inner loop feedback signal, are successfully estimated. However, their work suffers from two major drawbacks: first, an LCL filter, instead of a commonly used LC filter, is employed at the output of the inverter. With an LCL filter, the output inductor increases the converter output impedance, and consequently the harmonic voltage, when the load is distorted. Second, the load current is measured in their work, however in view of the inverter overcurrent protection, measurement of the inverter current is necessary in practice, even if it is not directly included in the control loops. Recently, a simple double-loop control algorithm with proportional controllers in both voltage and current loops is proposed, which replaces the load voltage sensor with an estimation algorithm based on the Kalman filter, while both inverter and load currents are measured directly [16].

In this paper, a modified multi-loop control method with the minimal sensors is proposed for the single phase stand-alone inverter. The multi-loop control scheme uses two estimated variables as feedback signals for the control loops. The outer loop regulates the output voltage via a proportional-resonant (PR) controller, which ensures zero steady-state error tracking performance of the 50 Hz reference signal. The inner loop actively damps the possible resonances due to the LC filter, and compensates the load disturbances through regulating the capacitor current. For this purpose, only the inverter current is measured, which is required for both control and protection purposes, then

the load voltage, and the load current are estimated by the Kalman filter, and the gradient descent adaptive control, respectively. Consequently, the filter capacitor current, which is the inner loop feedback variable, is calculated by the Kirchhoff's current law. Therefore, in principle, the proposed control scheme requires only one current sensor to measure the inverter current for both control and protection purposes. In Sections 4, and 5, the use of the Kalman filter, and the gradient descent adaptive control for operation of the multi-loop stand-alone inverter with only one sensor in the circuit is suggested.

## 2 System modelling

The schematic diagram of the power circuit of the single phase stand-alone inverter with output LC filter is shown in Fig. 1a.

The parameters of the converter circuit are summarised in Table 1. Based on Fig. 1a, a mathematical model, describing the dynamics of the stand-alone inverter can be derived as

$$v = r_L i_L + L \frac{di_L}{dt} + v_O \quad (1)$$

$$i_L = i_O + C \frac{dv_O}{dt} \quad (2)$$

where  $v$ , and  $v_O$  are the output voltage of the inverter, and the load voltage, respectively, and  $i_L$ , and  $i_O$  are the filter (inverter), and load currents, respectively. Based on (1), and (2), and considering that the switching frequency is much higher than the fundamental frequency, the averaged switching model (ASM) of the inverter can be obtained as Fig. 2a [16].

Equations (1), and (2) are rewritten as a state space system as

$$\begin{bmatrix} \dot{i}_L \\ \dot{v}_O \end{bmatrix} = \underbrace{\begin{bmatrix} -\frac{r_L}{L} & -\frac{1}{L} \\ \frac{1}{C} & 0 \end{bmatrix}}_A \begin{bmatrix} i_L \\ v_O \end{bmatrix} + \underbrace{\begin{bmatrix} \frac{1}{L} & 0 \\ 0 & -\frac{1}{C} \end{bmatrix}}_B \begin{bmatrix} v \\ i_O \end{bmatrix} \quad (3)$$

A discrete-time model of the system is readily obtained from (3) by assuming a sampling time  $T_s$  [13], as

$$\begin{bmatrix} i_L(k+1) \\ v_O(k+1) \end{bmatrix} = A_d \begin{bmatrix} i_L(k) \\ v_O(k) \end{bmatrix} + B_d \begin{bmatrix} v(k) \\ i_O(k) \end{bmatrix} \quad (4)$$

**Table 1** System parameters

Parameter	Description	Value
$C$	filter capacitance	25 $\mu\text{F}$
$L$	filter inductance	3.7 mH
$r_L$	filter resistance	0.2 $\Omega$
$V_{dc}$	DC link voltage	250 V
$V_o$	output voltage, rms	110 V
$f_s$	sampling/switching frequency	20 kHz
$f$	fundamental frequency	50 Hz
$S$	nominal power	600 VA

where

$$A_d = \mathfrak{S}^{-1}[(sI - A)^{-1}] \simeq I + AT_s = \begin{bmatrix} 1 - \frac{r_L T_s}{L} & -\frac{T_s}{L} \\ \frac{T_s}{C} & 1 \end{bmatrix},$$

$$B_d = \int_0^{T_s} A_d(T - \tau) B d\tau \simeq BT_s = \begin{bmatrix} \frac{T_s}{L} & 0 \\ 0 & -\frac{T_s}{C} \end{bmatrix}.$$

## 3 Control of stand-alone inverter

### 3.1 Suggested control structure

Fig. 2b shows the suggested dual-loop control scheme. An outer loop with the PR controller regulates the output voltage, while the capacitor current is selected as the feedback signal in the inner control loop. It is demonstrated that the capacitor current feedback brings better disturbance rejection capability than the inductor or load current feedback [1, 18–20]. However, the filter capacitor current feedback scheme cannot incorporate inverter overcurrent protection. To tackle this problem, instead of the capacitor current, the inductor current is measured directly for both feedback control, and overcurrent protection. It will be shown in the next sections that the extra sensor for the capacitor current can be replaced by an estimation algorithm. Moreover, the output voltage sensor can be eliminated by using an appropriate voltage estimator. Besides, in the suggested scheme a voltage feedforward path is added to reduce the control effort, and improve the system robustness [16].

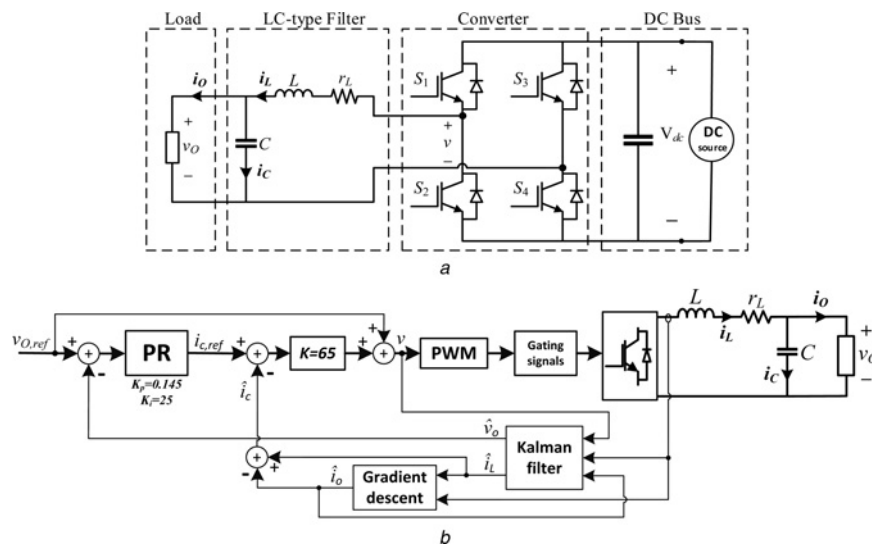


**Fig. 1** Schematic diagram of the

a Power stage of the single phase stand-alone inverter

b Proposed control system in presence of load voltage and current estimators

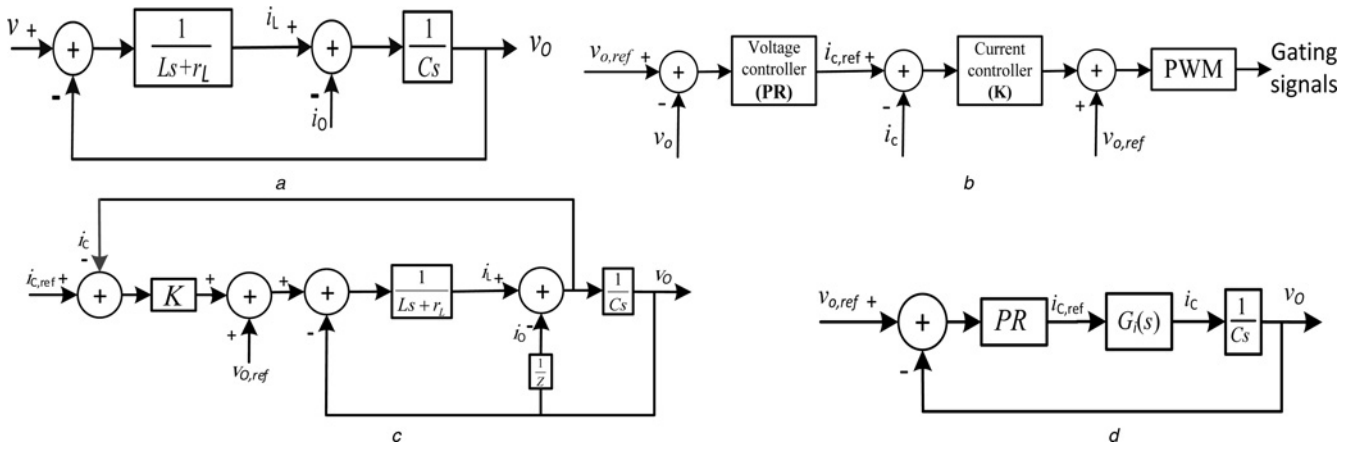


**Fig. 2** Block diagram of the

- a ASM of stand-alone inverter
- b Multi-loop control system for stand-alone inverter
- c Inner current control loop
- d Simplified proposed control system

### 3.2 Controller parameters design

The model of the inverter with the inner current control loop is shown in Fig. 2c, where  $Z$  is the load impedance [16]. By using a simple proportional controller, the system analysis, and the controller design are significantly simplified, and at the same time, the problem of phase delay at the fundamental frequency, associated to the PI controllers, is avoided.

The closed loop transfer function is obtained as

$$G_i(s) = \frac{i_c}{i_{c,ref}} = \frac{ZCKs}{ZCLs^2 + (ZC(r_L + K) + L)s + r_L} \quad (5)$$

The current controller bandwidth is chosen to be one-tenth of the switching frequency ( $f_s$ ), i.e.

$$\omega_{bi} = 2\pi(0.1 \times f_s) = 2\pi(0.1 \times 20 \text{ kHz}) \simeq 12.5 \text{ krad/s} \quad (6)$$

Consequently,  $K$  is determined from (5), by solving  $|G_i(j\omega_{bi})|^2 = 1/2$ , to be about 65.

The next step is to tune the parameters of the voltage feedback loop. Fig. 2d shows the simplified block diagram of the proposed control system, in which the inner current control loop is replaced by  $G_i(s)$  from (5).

The transfer function of a gain-limited PR controller is [21]

$$G_{PR}(s) = K_p + \frac{2K_i\omega_c s}{s^2 + 2\omega_c s + (2\pi f)^2} \quad (7)$$

where  $K_p$ , and  $K_i$  are the proportional and integral (resonator) gains, respectively, and  $\omega_c$  is the frequency bandwidth around the resonance frequency, which is commonly selected in the range of 5 to 10 rad/s [21, 22], and in our application is chosen to be 5 rad/s that showed the best results for our application.

According to Monfared *et al.* [1], under light loads, the phase margin (PM) and the closed loop stability are slightly reduced, therefore the voltage loop PR controller is tuned under light load conditions ( $Z$  tends to  $\infty$ ). This assumption not only simplifies the analysis, but also is conservative and ensures stability for all operating conditions. Moreover, it is shown that the PR controller is mathematically equivalent to a synchronous reference frame PI (SRF-PI) controller [23]. Hence, the parameters of the PR controller are designed according to the recommendations of Monfared *et al.* [1], which proposes a frequency domain design approach for the SRF-PI controller.

The following analysis to determine  $K_p$  is based on the assumption that the integral gain has almost no effect on the voltage regulation dynamics. However, when attending the system stability, the effect of  $K_i$  and  $K_p$  will be considered simultaneously. Using the aforementioned assumption, the transfer function of the closed loop system under light loads can be written as

$$G(s) = \frac{v_o}{v_{o,ref}} = \frac{KK_p}{LCs^2 + C(r_L + K)s + KK_p} \quad (8)$$

The choice of system bandwidth is a compromise between the transient response, and the disturbance rejection requirement. In practice, a value in the range of 10 times the fundamental frequency, and one-tenth the switching frequency may be chosen to get both fast dynamics, and switching noise immunity. For the inverter under study, a value of 1.25 kHz is decided for the control bandwidth which is in the middle of the desired range. Evaluating (8) at  $\omega_{bv} = 2\pi \times 1.25 \text{ kHz} \simeq 7.85 \text{ krad/s}$ , by solving  $|G(j\omega_{bv})|^2 = 1/2$ , yields  $K_p = 0.145$ .

Deciding the proportional gain, now the integral gain is determined from the closed loop stability analysis. The system characteristic equation, with considering the effect of  $K_i$  and  $K_p$  simultaneously, is obtained as

$$s^4 + \frac{C(r_L + K) + 2\omega_c LC}{LC} s^3 + \frac{2\omega_c C(r_L + K) + KK_p + LC(2\pi f)^2}{LC} s^2 + \frac{(r_L + K)C(2\pi f)^2 + 2K\omega_c(K_p + K_i)}{LC} s + \frac{KK_p(2\pi f)^2}{LC} = 0. \quad (9)$$

Applying the Routh–Hurwitz stability criterion to the system characteristic polynomial of (9), gives the stability limit as

$$K_i \leq K_p \left[ \frac{K}{2L\omega_c} - 1 \right] \quad (10)$$

This establishes an upper limit for  $K_i$  in terms of  $L$ ,  $K$ ,  $\omega_c$ , and  $K_p$ , which in our case is  $K_p \times [K/2L\omega_c - 1] \simeq 250$ . Sufficiently far from the limit,  $K_i$  is chosen to be 25 in our work.

The open-loop bode plot is shown in Fig. 3, in which the resonant term is set to zero due to its negligible effect on the bandwidth. This figure indicates that the PM is more than  $72^\circ$ , which is quite enough for most power electronic applications. However, this value for PM cannot be achieved in practice, due to some practical effects, such as

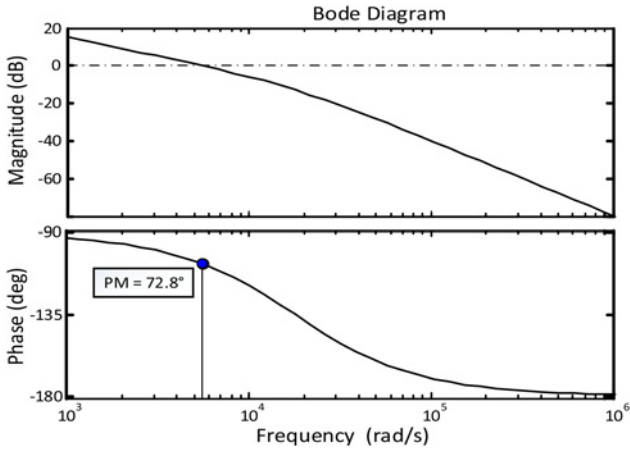


Fig. 3 Open-loop bode plot of the voltage control loop ( $K_i = 0$ )

control and pulse-width modulation (PWM) delays, and dynamics of estimators. Indeed, digital control systems impose an additional time delay in the control loop. This delay corresponds to the digital sampling, program computation time, and PWM register update and results in one and half PWM period delay in digital execution of the control algorithm [1]. Besides, the delay of estimators must be considered. Assuming a one sampling period delay for estimators, the overall effect of digital implementation and estimation dynamics can be simplified as a two and half sampling period delay. In this work, the gain crossover frequency of the open loop system ( $\omega_c$ ) is about 5 krad/s, therefore each sampling period delay decreases the PM by about  $14^\circ$ . Indeed, the digital system delay does not affect the magnitude of the system transfer functions; however the PM is reduced as  $\Delta PM = -\omega_c T_d$ , when a time delay of  $T_d$  contributes to the control loop [1]. Therefore, the new PM is about  $37^\circ$  and still adequate to ensure the system stability.

#### 4 Output voltage estimation with Kalman filter

The Kalman filter is a set of mathematical equations that provides an efficient computational means to estimate the states of a process ( $x$ ), in a way that minimises the mean of the squared error [24]. In this work, the Kalman filter is used for estimation of the output voltage. For this purpose, by measurement of the filter inductor current, estimates of state variables are obtained.

Assuming that  $x_k = [i_L(k) \ v_O(k)]^T$ , and  $u_k = [v(k) \ i_O(k)]^T$ , the stochastic difference equations of the studied system in (4), with the measurement  $z$ , are expressed as

$$\underbrace{\begin{bmatrix} i_L(k+1) \\ v_O(k+1) \end{bmatrix}}_{x_{k+1}} = A_d \underbrace{\begin{bmatrix} i_L(k) \\ v_O(k) \end{bmatrix}}_{x_k} + B_d \underbrace{\begin{bmatrix} v(k) \\ i_O(k) \end{bmatrix}}_{u_k} + w_k \quad (11)$$

$$z_k = Hx_k + v_k.$$

The random variables  $w_k$ , and  $v_k$  represent the process, and measurement noise, respectively.

The Kalman filter has two set of equations: the time update, and the measurement update. The time update equations predict the states and error covariance matrix ( $P$ ) one sample in advance to obtain the a priori estimate for the next time step. The measurement update equations correct the predicted states and error covariance matrix through a feedback correction scheme from actual measurement ( $z$ ), resulting in an improved a posteriori estimate. For the system described by (11), the time update equations are

$$\hat{x}_k^- = A_d \hat{x}_{k-1} + B_d u_{k-1} \quad (12)$$

$$P_k^- = A_d P_{k-1} A_d^T + Q \quad (13)$$

and measurement update equations are

$$K_k = P_k^- H^T (H P_k^- H^T + R)^{-1} \quad (14)$$

$$\hat{x}_k = \hat{x}_k^- + K_k (z_k - H \hat{x}_k^-) \quad (15)$$

$$P_k = (I - K_k H) P_k^- \quad (16)$$

where  $H = [1 \ 0]$ ,  $K_k$  is the Kalman gain, and  $P_k^-$ ,  $P_k$ ,  $Q$ , and  $R$  are the covariances matrices of a priori estimate error, a posteriori estimate error, process noise, and measurement noise, respectively, defined as

$$P_k^- = E[(x_k - \hat{x}_k^-)(x_k - \hat{x}_k^-)^T], \quad Q = E[w_k w_k^T] \quad (17)$$

$$P_k = E[(x_k - \hat{x}_k)(x_k - \hat{x}_k)^T], \quad R = E[v_k v_k^T].$$

It should be noted that we need the initial values for states ( $\hat{x}_0$ ) and error covariance matrix ( $P_0$ ), which are usually set to zero. Moreover, it is a common practice to assume the noise covariance matrices as unity matrices [25]. Therefore,  $Q$  and  $R$  are assumed to be

$$Q = \begin{bmatrix} 1 & 0 \\ 0 & 1 \end{bmatrix} \quad (18)$$

$$R = 1 \quad (19)$$

After each time and measurement update pair, the process is repeated with the previous a posteriori estimate used to predict the new a priori estimate [26].

Finally, as already shown in Fig. 1b, the Kalman algorithm receives the measured state variable  $i_L$  and the input variables  $v$  and  $\hat{i}_O$  to estimate the other state variable ( $\hat{v}_O$ ). Moreover, it calculates the estimated/filtered version of the measured inverter current ( $\hat{i}_L$ ), from the developed converter model, which will be used to estimate the load current through the gradient descent algorithm.

It should be noted that the input vector of  $u$  consists of the inverter output voltage, and the load current. Evidently, the inverter output voltage can be replaced by its reference, and therefore, no extra measurement is needed. Moreover, the load current is estimated by the gradient descent adaptive controller, which will be described in the next section.

#### 5 Output current estimation with gradient descent

This is not possible to use the Kalman filter to estimate the output current too; because the added equation for this variable will change the observability of the system. Therefore, the gradient descent adaptive control is adopted in conjunction with the estimate provided by the Kalman filter as a means to estimate the output current, which is then used by the Kalman algorithm. The gradient descent, also known as the steepest descent, is a first-order optimisation algorithm, which searches for the minimum of a function of many variables [27]. In our problem, the difference between the actual and estimated filter inductor current is used for the estimation of the output current. For this purpose, the cost function, and equations of estimation are proposed as [13, 19]

$$e_o(k) = i_L(k) - \hat{i}_L(k) \quad (20)$$

$$f(k) = \frac{1}{2} (i_L(k) - \hat{i}_L(k))^2 = \frac{1}{2} e_o^2(k) \quad (21)$$

$$\hat{i}_O(k+1) = \hat{i}_O(k) - \lambda \nabla f(k) = \hat{i}_O(k) - \lambda e_o(k) \quad (22)$$

where  $f(k)$  is the quadratic cost function,  $\lambda$  is a positive gain, which controls the speed of convergence and stability of the controller, and  $\nabla f(k)$  is the gradient of the cost function with respect to the filter inductor current, and as previous, the quantities with a  $\hat{\cdot}$  are the estimated ones.

**Table 2** Comparative results for the converter operation with and without the estimators

Loading condition	$V_{or}$ rms	$i_o$			with estimators				without estimators		
		rms	CF	THD, %	THDv, %	Voltage amplitude error, %	Voltage phase error, degree	THDv, %	Voltage amplitude error, %	Voltage phase error, degree	
nominal resistive load	Sim. (Fig. 4)	110.2	5.5	1.41	0.04	0.04	2.50	<1	0.03	1.54	<0.5
	Exp. (Fig. 7)	111.4	5.3	1.45	1.9	2.3	3.85	<1	1.9	2.56	<0.5
no load	Sim. (Fig. 4)	110.2	0	–	–	0.06	2.66	<1	0.03	1.54	<0.5
	Exp. (Fig. 8)	111.2	0	–	–	1.6	3.85	<1	1.4	2.56	<0.5
highly non-linear load	Sim. (Fig. 4)	110.2	4.4	3.12	88.5	1.77	4.42	<1	1.72	3.22	<0.5
	Exp. (Fig. 7)	110.8	4.7	3.51	75	4.6	6.41	<1	4.4	4.50	<0.5

The selection of the gain  $\lambda$  is conducted according to the Lyapunov theory. The proposed Lyapunov function can be  $e_o^2(k)$ , which must satisfy the criteria of the Lyapunov theory:

- (i)  $e_o^2(k) > 0$ , that the square function satisfies this condition.
- (ii)  $\Delta e_o^2(k) < 0$ , that to satisfy requirement of this criterion, the inequality of (23) must hold.

$$e_o^2(k+1) - e_o^2(k) < 0 \Rightarrow f(k+1) < f(k) \quad (23)$$

As shown in [28], if  $\lambda < (1/L(\nabla f))$ , the inequality of (23) will be established, where  $L(\nabla f)$  is known as the Lipschitz constant of

$\nabla f(k)$ , and has the maximum of the derivatives at all points. In this paper,  $\nabla f(k)$  is  $e_o(k)$ , and therefore  $L(\nabla f) = 1$ , which sets  $\lambda < 1$ . In our work,  $\lambda$  is chosen to be 0.5.

Compared with the procedure already reported in [19], in this paper, a modification to (23) is proposed, which is realised by substituting  $\hat{i}_o(k)$  with the average of  $i_o^*(k)$  and  $\hat{i}_o(k)$ , where  $i_o^*(k)$  is obtained by the KCL in the output node, as

$$i_o^*(k) = i_L(k) - C \frac{\hat{v}_O(k) - \hat{v}_O(k-1)}{T_s} \quad (24)$$

This modification increases the convergence speed, the accuracy of estimation, and especially the stability of the system. However, at

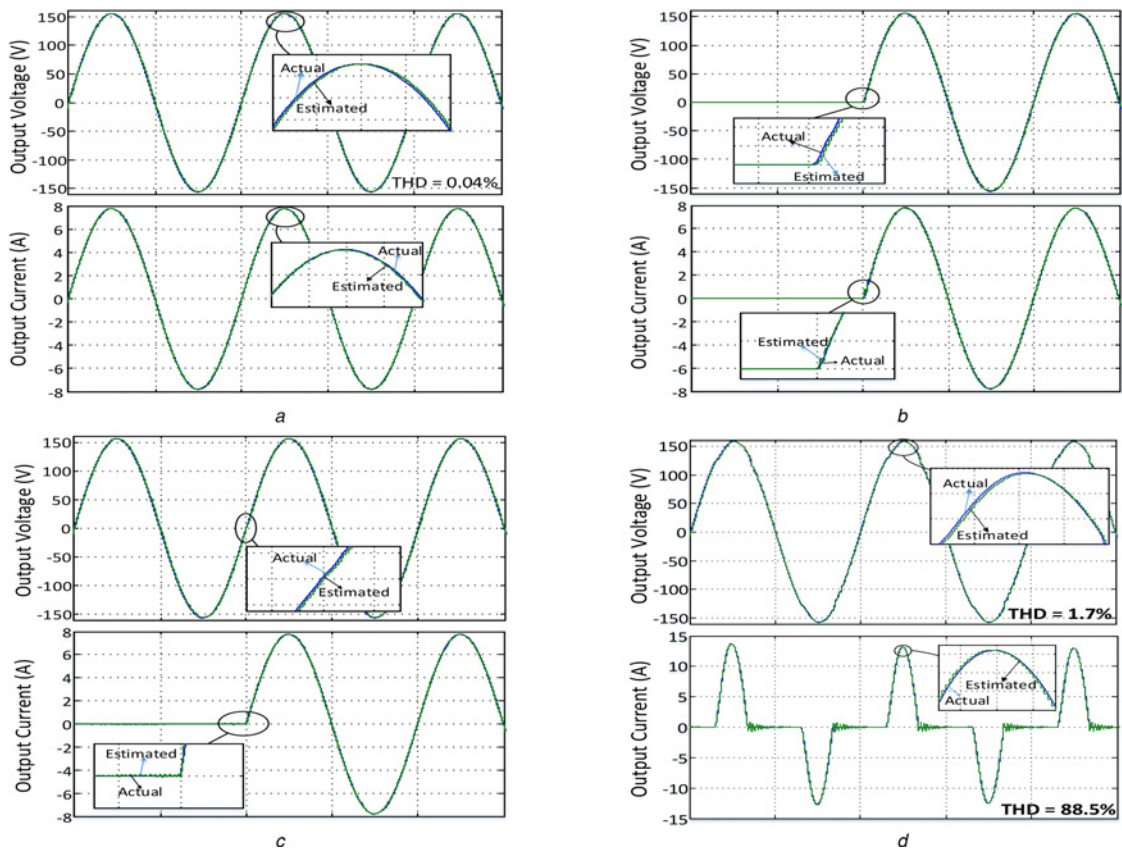


**Fig. 4** Measured and estimated output voltage and current

- a Under the nominal linear load
- b Transient from no load to full load
- c Transient on zero power command startup
- d Under a highly non-linear load

the end of Section 3, the stability margin was examined with the simplified assumption that the estimators can be simply modelled as a unit delay, the stability of overall system, including the dynamics of estimators, is discussed in details in Appendix 1. Moreover, the controllability and observability of overall system is investigated in Appendix 2.

## 6 Performance evaluation

### 6.1 Simulation experiments

To confirm the performance of the proposed multi-loop load parameter sensorless control algorithm, the single-phase inverter system of Fig. 1b has been extensively investigated using MATLAB/SIMULINK simulations. The simulation parameters are listed in Table 1. Moreover, the steady-state performance of the double-loop control scheme of Fig. 1b without the estimators (with direct measurement of load voltage and current) is compared with the load sensorless operation with numerical results in Table 2.

Fig. 4a shows the steady-state measured and estimated output voltage and current for the nominal linear load. No steady-state phase and amplitude error can be recognised, and the estimated load voltage and current track the actual ones accurately. The total harmonic distortion (THD) of output voltage is 0.04%.

Figs. 4b and c present the transient performance of the system under no load to full load, and zero power command startup transitions. It can be seen that the transient dies out rapidly, and the estimation error remains almost unchanged during the load change or startup. This excellent transient performance is achieved because the capacitor current changes instantaneously with the load current change, irrespective of the inductor current.

The performance of the proposed control scheme was evaluated under a highly non-linear load, and the results are shown in Fig. 4d. The non-linear load, designed according to IEC 62040-3 standard (Annex E), consists of a 2  $\Omega$  resistor in series with a diode rectifier bridge feeding a 3400  $\mu\text{F}$  capacitor in parallel with a 45  $\Omega$  resistor. One can see in Fig. 4d that while the load current is highly distorted, with a THD of about 90%, the voltage waveform remains sinusoidal (THD=1.7%). It is worth mentioning that the standard limit for the voltage THD under this condition is 8% [29]. Moreover, the estimated waveforms track the actual ones perfectly.

In practice, the parameters of the LC filter may not be exactly known or may vary as a consequence of varying operating conditions and aging. The performance of the control system without the estimators, in terms of the PM and the control bandwidth, considering mismatches in the  $L$  and  $C$  values, is investigated, and the results are depicted in Fig. 5. Fig. 5a shows that  $L$  and  $C$  uncertainties lead to PM variations; however for a wide range of mismatches the PM remains satisfactory. Moreover, Fig. 5b shows that the  $\omega_{bv}$  mainly remains unchanged with inductance mismatches, however the capacitance uncertainties lead to large bandwidth variations, especially if the capacitor value is underestimated, then a remarkable increase in the voltage loop bandwidth is expected. This may cause the system response to be highly oscillatory and even unstable. The performance of the estimators in presence of mismatches is also investigated, and the results are depicted in Fig. 6. This figure shows that mismatches in the  $L$  and  $C$  values, have almost no effect on the THD of output voltage and the operation of the current estimator. Moreover, Fig. 6a shows that while the voltage estimator acts properly in presence of considerable inductance mismatches, but the capacitance uncertainties have a high impact on the operation of the voltage estimator.

This is caused by the significant role of the capacitor value compared with the inductor value in the state-space equations of the Kalman filter algorithm. As seen in (27),  $L$  and  $C$  appear as  $T_s/L$  and  $T_s/C$  terms in the voltage estimation equation, which in our application are 0.013 and 2, respectively. This is the main reason that the voltage estimator is more susceptible to capacitor mismatches than the inductor mismatches. Therefore, the proposed method requires an accurate recognition of the filter capacitor value.

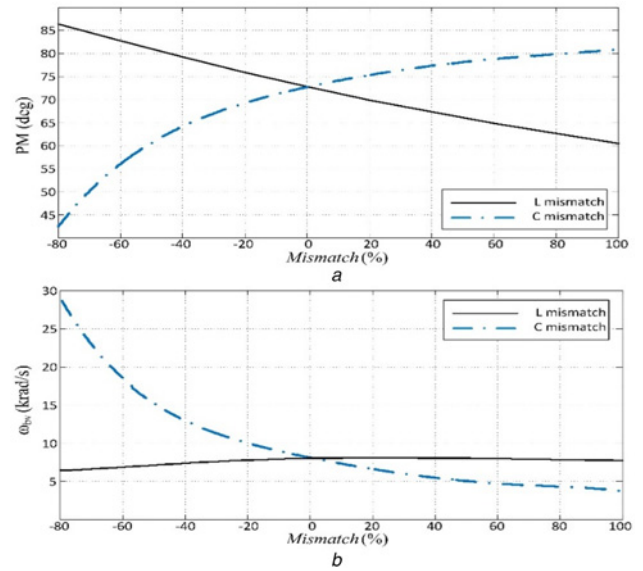


Fig. 5 Effect of  $L$  and  $C$  mismatches (in per cent) on

a PM  
b Closed-loop control bandwidth

### 6.2 Practical implementation

A digitally controlled single-phase inverter was developed to verify the conclusions of the simulation studies. The experimental platform

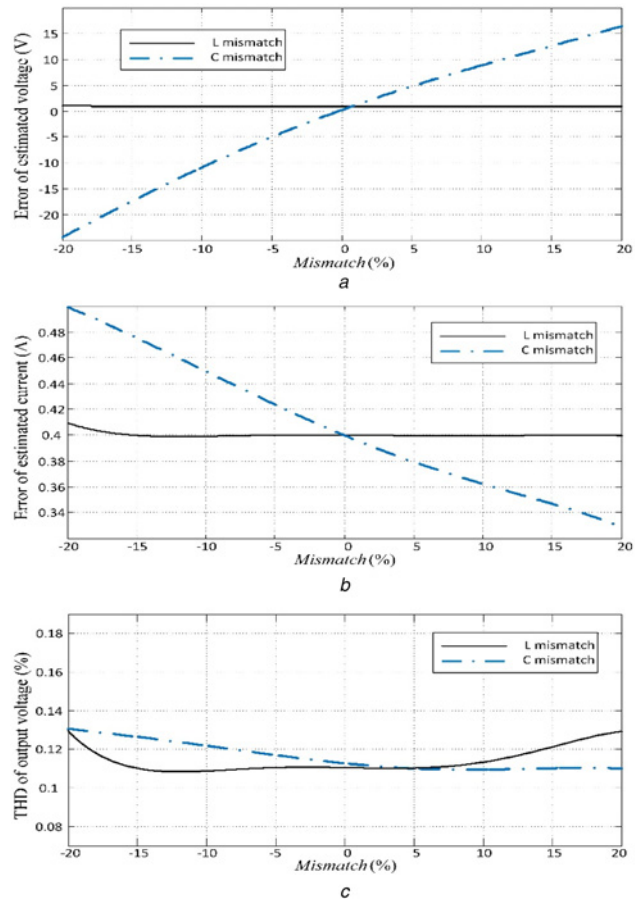
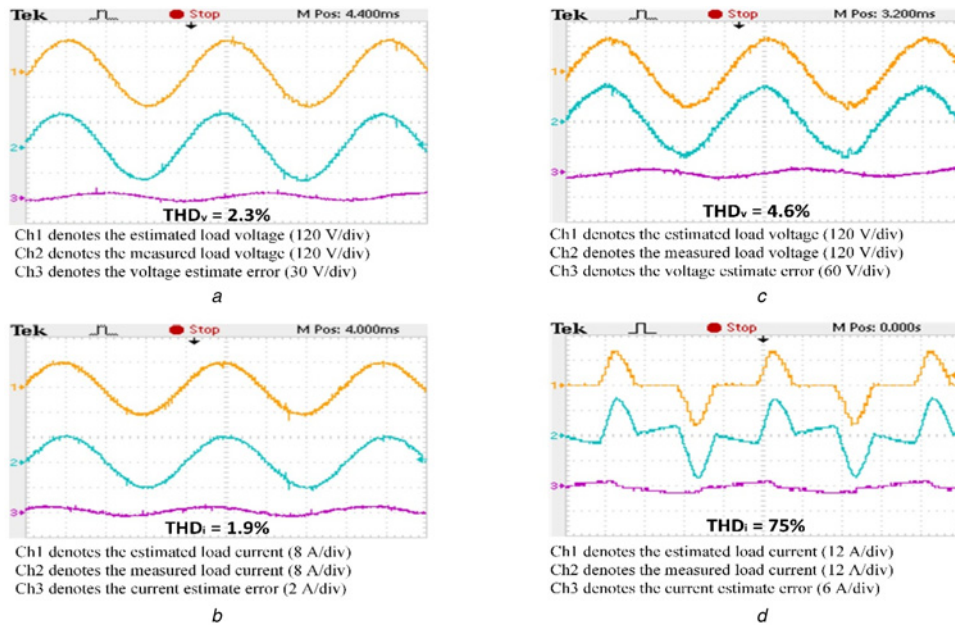


Fig. 6 Effect of  $L$  and  $C$  mismatches on

a Error of estimated voltage  
b Error of estimated current  
c THD of output voltage



**Fig. 7** Steady-state waveforms for  
*a* and *b* the nominal resistive load ( $R = 20 \Omega$ )  
*c* and *d* the highly non-linear load

consists of a dc-link, a full-bridge IGBT intelligent power module, an output LC filter, measurement, and gate drive circuits.

The dc-link is fed from a three-phase diode-bridge rectifier. The control algorithm is implemented by using a TMS320F28335 digital signal processor from Texas Instruments. The experimental system parameters are the same as the simulation studies. Again, the converter operation with and without the estimators is compared numerically in Table 2.

In the first study, the steady-state behaviour of the proposed controller under the nominal resistive load is investigated, and the results are shown in Figs. 7*a* and *b*, where the load voltage and current, as well as, the estimation errors are depicted. The

performance of both estimators is excellent. It is also shown that the output voltage is sinusoidal with a very low distortion.

In another study, as a worst case operation, a highly non-linear load similar to the simulated one is connected to the inverter output and the results are shown in Figs. 7*c* and *d*. Here, the load voltage is still sinusoidal (THD = 4.6%), despite the highly distorted load current with a THD of about 75% and a crest factor of about 3.5:1.

Finally, the transient behaviour of the system for a load step change from no load to the nominal resistive load is shown in Figs. 8*a* and *b*. It can be seen that the output voltage is not affected by the change in the load, and the current regulator

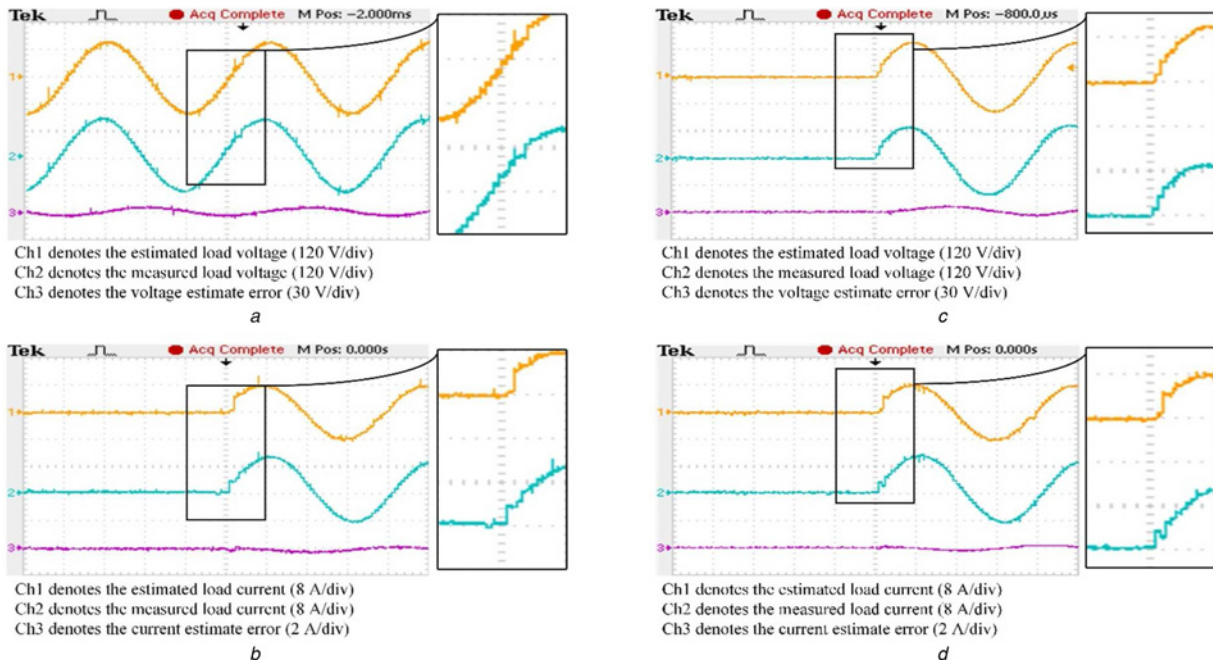


**Fig. 8** Transient waveforms for  
*a* and *b* no load to nominal load step change  
*c* and *d* zero power startup command

dynamic is fast, and smooth. In addition, the startup transient behaviour of the system is shown in Figs. 8c and d. In this case, all transients, including the estimation and control of the output voltage, die in less than a quarter of cycle.

As already stated, the quality of the voltage waveform in terms of THD and the steady-state amplitude and phase errors for different loading conditions are summarised in Table 2. The operation with and without the estimators are compared in simulations and experiments. The simulation and experimental results agree. The increase of the output voltage THD with the estimators compared with the direct measurement case is around 10%. The deviation of the output voltage phase from its reference is negligible, while the deviation of the output voltage amplitude from its reference, for the worst loading condition, is still below 5% and 6.5% for operation with direct measurement and estimation of load parameters, respectively.

## 7 Conclusion

The feasibility and performance of a load parameter sensorless dual-loop control method for the single-phase stand-alone inverter with the output LC filter have been investigated. This control topology involves two main control loops: an output voltage control loop, in which the feedback variable is estimated by the Kalman filter, and a capacitor current control loop, in which the feedback variable is estimated by the gradient descent adaptive controller. In principle, the proposed control scheme requires only one current sensor to measure the inverter current for control and protection purposes. The proposed control and estimation strategy can supply different load types with negligible control error and harmonic distortions in the output voltage, however it requires an accurate identification of the filter capacitor value.

## 8 References

- 1 Monfared, M., Golestan, S., Guerrero, J.M.: 'Analysis, design, and experimental verification of a synchronous reference frame voltage control for single-phase inverters', *IEEE Trans. Ind. Electron.*, 2014, **61**, (1), pp. 258–269
- 2 Heng, D., Oruganti, R., Srinivasan, D.: 'A simple control method for high-performance UPS inverters through output-impedance reduction', *IEEE Trans. Ind. Electron.*, 2008, **55**, (2), pp. 888–898
- 3 Lidozzi, A., Ji, C., Solero, L., et al.: 'Resonant-repetitive combined control for stand-alone power supply units', *IEEE Trans. Ind. Appl.*, 2015, **51**, (6), pp. 4653–4663
- 4 Liu, T., Wang, D.: 'Parallel structure fractional repetitive control for PWM inverters', *IEEE Trans. Ind. Electron.*, 2015, **62**, (8), pp. 5045–5054
- 5 Chen, Y., Luo, A., Shuai, A., et al.: 'Robust predictive dual-loop control strategy with reactive power compensation for single-phase grid-connected distributed generation system', *IET Power Electron.*, 2013, **6**, (7), pp. 1320–1328
- 6 Niroomand, M., Karshenas, H.R.: 'Hybrid learning control strategy for three-phase uninterruptible power supply', *IET Power Electron.*, 2011, **4**, (7), pp. 799–807
- 7 Kwak, S., Mun, S.: 'Model predictive control methods to reduce common-mode voltage for three-phase voltage source inverters', *IEEE Trans. Power Electron.*, 2015, **30**, (9), pp. 5019–5035
- 8 Yaramasu, V., Rivera, M., Narimani, M., et al.: 'Model predictive approach for a simple and effective load voltage control of four-leg inverter with an output LC filter', *IEEE Trans. Ind. Electron.*, 2014, **61**, (10), pp. 5259–5270
- 9 Lim, J.S., Park, C., Han, J., et al.: 'Robust tracking control of a three-phase DC-AC inverter for UPS applications', *IEEE Trans. Ind. Electron.*, 2014, **59**, (1), pp. 4142–4151
- 10 Lee, T.S., Tzeng, K.S., Chong, M.S.: 'Robust controller design for a single-phase UPS inverter using  $\mu$ -synthesis', *Proc. Inst. Electr. Eng. Electr. Power Appl.*, 2004, **151**, (3), pp. 334–340
- 11 Komurcugil, H., Altin, N., Ozdemir, S., et al.: 'An extended lyapunov-function-based control strategy for single-phase UPS inverters', *IEEE Trans. Power Electron.*, 2015, **30**, (7), pp. 3976–3983
- 12 Tai, T.L., Chen, J.S.: 'UPS inverter design using discrete-time sliding-mode control scheme', *IEEE Trans. Ind. Electron.*, 2002, **49**, (1), pp. 67–75
- 13 Ahmed, K.H., Massoud, A.M., Finney, S.J., et al.: 'Autonomous adaptive sensorless controller of inverter-based islanded-distributed generation system', *IET Power Electron.*, 2009, **2**, (3), pp. 256–266
- 14 Lei, Q., Peng, F.Z., Yang, S.: 'Multiloop control method for high-performance microgrid inverter through load voltage and current decoupling with only output voltage feedback', *IEEE Trans. Power Electron.*, 2011, **26**, (3), pp. 953–960
- 15 Loh, P.C., Holmes, D.G.: 'Analysis of multiloop control strategies for LC/CL/LCL-filtered voltage-source and current-source inverters', *IEEE Trans. Ind. Appl.*, 2005, **41**, (2), pp. 644–654

- 16 Razi, R., Monfared, M.: 'Simple control scheme for single-phase uninterruptible power supply inverters with Kalman filter-based estimation of the output voltage', *IET Power Electron.*, 2015, **8**, (9), pp. 1817–1824
- 17 Li, Y.W.: 'Control and resonance damping of voltage-source and current-source converters with LC filters', *IEEE Trans. Ind. Electron.*, 2009, **56**, (5), pp. 1511–1521
- 18 Wai, R.J., Lin, C.Y., Wu, W.C., et al.: 'Design of backstepping control for high-performance inverter with stand-alone and grid-connected power-supply modes', *IET Power Electron.*, 2013, **6**, (4), pp. 752–762
- 19 Hasanzadeh, A., Edrington, C.S., Maghsoudlou, B., et al.: 'Multi-loop linear resonant voltage source inverter controller design for distorted loads using the linear quadratic regulator method', *IET Power Electron.*, 2012, **5**, (6), pp. 841–851
- 20 Vandoom, T.L., Ionescu, C.M., De Kooking, J.D.M., et al.: 'Theoretical analysis and experimental validation of single-phase direct vs. cascade voltage control in islanded microgrids', *IEEE Trans. Ind. Electron.*, 2013, **60**, (2), pp. 789–798
- 21 Zmood, D.N., Holmes, D.G.: 'Stationary frame current regulation of PWM inverters with zero steady-state error', *IEEE Trans. Power Electron.*, 2003, **18**, (3), pp. 814–822
- 22 Teodorescu, R., Blaabjerg, F., Liserre, M., et al.: 'Proportional-resonant controllers and filters for grid-connected voltage-source converters', *IEE Proc. Electron. Power Appl.*, 2006, **153**, (5), pp. 750–762
- 23 Zou, C., Liu, B., Duan, S., et al.: 'Stationary frame equivalent model of proportional-integral controller in dq synchronous frame', *IEEE Trans. Power Electron.*, 2014, **29**, (9), pp. 4461–4465
- 24 Simon, D.: 'Kalman filtering with state constraints: a survey of linear and nonlinear algorithms', *IET Power Electron.*, 2010, **4**, (8), pp. 1303–1318
- 25 Corriou, J.P.: 'Process control-theory and applications' (Springer-Verlag, London, 2004)
- 26 Welch, G., Bishop, G.: 'An introduction to the Kalman filter'. Technical Report TR 95-041, Department of computer science, University of North Carolina at Chapel Hill, 2004
- 27 Haykin, S.: 'Adaptive filter theory' (Prentice-Hall, Upper Saddle River, NJ, 1995, 3rd edn.)
- 28 Ghadimi, E., Shames, I., Johansson, M.: 'Multi-step gradient methods for networked optimization', *IEEE Trans. Signal. Proc.*, 2013, **61**, (21), pp. 5417–5429
- 29 Uninterruptible power systems (UPS) – Part 3: Method of specifying the performance and test requirements, Second edition 2011-3, International Standard IEC 62040-3

## 9 Appendices

### 9.1 Stability of overall system, including the dynamics of estimators

Assuming that the Kalman gain  $K_k = [K_1 \ K_2]^T$  is in its steady-state condition, then by substituting (12) in (15), the a posteriori estimate of state variables can be written as

$$\hat{x}_{k+1} = \begin{bmatrix} 1 - K_1 & 0 \\ -K_2 & 1 \end{bmatrix} (A_d \hat{x}_k + B_d u_k) + \begin{bmatrix} K_1 \\ K_2 \end{bmatrix} z_{k+1} \quad (25)$$

Substituting for  $A_d$  and  $B_d$  from (4) and expanding the result, yields

$$\begin{aligned} \hat{i}_L(k+1) &= (1 - K_1) \left( 1 - \frac{r_L T_s}{L} \right) \hat{i}_L(k) - (1 - K_1) \frac{T_s}{L} \hat{v}_O(k) \\ &\quad + K_1 \left( 1 - \frac{r_L T_s}{L} \right) i_L(k) - K_1 \frac{T_s}{L} v_O(k) + v(k) \end{aligned} \quad (26)$$

$$\begin{aligned} \hat{v}_O(k+1) &= \left( -K_2 \left( 1 - \frac{r_L T_s}{L} \right) + \frac{T_s}{C} \right) \hat{i}_L(k) \\ &\quad + \left( K_2 \frac{T_s}{L} + 1 \right) \hat{v}_O(k) - \frac{T_s}{C} \hat{i}_O(k) \\ &\quad + K_2 \left( 1 - \frac{r_L T_s}{L} \right) i_L(k) - K_2 \frac{T_s}{L} v_O(k) \end{aligned} \quad (27)$$

Moreover, the dynamic equation of the gradient descent is obtained by substituting (24) in (22) as

$$\begin{aligned} \hat{i}_O(k+1) &= \frac{1}{2} (\hat{i}_O(k) + i_L(k)) - \frac{1}{2} \frac{C}{T_s} (\hat{v}_O(k) - \hat{v}_O(k-1)) \\ &\quad - \lambda (i_L(k) - \hat{i}_L(k)) \end{aligned} \quad (28)$$



With the assumption that  $\hat{v}_O(k) = \hat{v}_O(k-1)$ , (28) simplifies to

$$\hat{i}_O(k+1) = \frac{1}{2}\hat{i}_O(k) + \left(\frac{1}{2} - \lambda\right)i_L(k) + \lambda\hat{i}_L(k) \quad (29)$$

Finally, the state space equations of system with considering the equations of the estimators ((26), (27), and (29)) can be concluded as (see (30))

To ensure the BIBO stability of discrete time systems, all eigenvalues must lie inside the unit circle in the complex plane.

The magnitudes of eigenvalues of system dynamics matrix  $A_{Od}$  calculated with the system parameters, are

$$\begin{aligned} &0.3770, \\ &0.5055, \\ &0.9943, \\ &0.9970, \\ &0.9993 \end{aligned}$$

which are all inside the stability region. Therefore, the overall system considering the equations of the estimators is asymptotically stable.

## 9.2 Observability and controllability of overall system, including the dynamics of estimators

The state space equations of system with considering the equations of the estimators is obtained as (30). Hence, controllability and observability of overall system can be obtained from below matrices.

$$S = [B_{Oc} \quad A_{Oc}B_{Oc} \quad A_{Oc}^2B_{Oc} \quad A_{Oc}^3B_{Oc} \quad A_{Oc}^4B_{Oc}] \quad (31)$$

$$V = \begin{bmatrix} C_{od} \\ C_{od}A_{od} \\ C_{od}A_{od}^2 \\ C_{od}A_{od}^3 \\ C_{od}A_{od}^4 \end{bmatrix} \quad (32)$$

The matrices (31), and (32) have full rank. As a result, the overall dynamic system is observable and controllable.

$$\begin{aligned} \begin{bmatrix} i_L(k+1) \\ v_O(k+1) \\ \hat{i}_O(k+1) \\ \hat{i}_L(k+1) \\ \hat{v}_O(k+1) \end{bmatrix} &= \underbrace{\begin{bmatrix} 1 - \frac{r_L T_s}{L} & -\frac{T_s}{L} & 0 & 0 & 0 \\ \frac{T_s}{C} & 1 & -\frac{T_s}{C} & 0 & 0 \\ 0.5 - \lambda & 0 & 0.5 & \lambda & 0 \\ K_1 \left(1 - \frac{r_L T_s}{L}\right) & -K_1 \frac{T_s}{L} & 0 & (1 - K_1) \left(1 - \frac{r_L T_s}{L}\right) & -(1 - K_1) \frac{T_s}{L} \\ K_2 \left(1 - \frac{r_L T_s}{L}\right) & -K_2 \frac{T_s}{L} & -\frac{T_s}{C} & -K_2 \left(1 - \frac{r_L T_s}{L}\right) + \frac{T_s}{C} & K_2 \frac{T_s}{L} + 1 \end{bmatrix}}_{A_{Od}} \begin{bmatrix} i_L(k) \\ v_O(k) \\ \hat{i}_O(k) \\ \hat{i}_L(k) \\ \hat{v}_O(k) \end{bmatrix} + \underbrace{\begin{bmatrix} \frac{T_s}{L} & 0 \\ 0 & 0 \\ 0 & 0 \\ 1 & 0 \\ 0 & 0 \end{bmatrix}}_{B_{Od}} \begin{bmatrix} v(k) \\ i_O(k) \end{bmatrix} \quad (30) \\ \begin{bmatrix} \hat{i}_O(k+1) \\ \hat{v}_O(k+1) \end{bmatrix} &= \underbrace{\begin{bmatrix} 0.5 - \lambda & 0 & 0.5 & \lambda & 0 \\ K_2 \left(1 - \frac{r_L T_s}{L}\right) & -K_2 \frac{T_s}{L} & -\frac{T_s}{C} & -K_2 \left(1 - \frac{r_L T_s}{L}\right) + \frac{T_s}{C} & K_2 \frac{T_s}{L} + 1 \end{bmatrix}}_{C_{Od}} \begin{bmatrix} \hat{i}_O(k) \\ \hat{v}_O(k) \end{bmatrix} + \underbrace{\begin{bmatrix} 0 & 0 \\ 0 & 0 \end{bmatrix}}_{D_{Od}} \begin{bmatrix} v(k) \\ i_O(k) \end{bmatrix} \end{aligned}$$